

# Regulation of membrane scission in yeast endocytosis

Deepikaa Menon and Marko Kaksonen\*

\*For correspondence:  
Marko.Kaksonen@unige.ch

Department of Biochemistry and National Centre of Competence in Research,  
Chemical Biology, University of Geneva, Geneva, Switzerland

## Abstract

During clathrin-mediated endocytosis, flat plasma membrane is transformed into an invagination and eventually into an endocytic vesicle. In mammalian cells, the transition from invagination to vesicle is driven by the GTPase dynamin together with BAR domain proteins. In yeast cells, a heterodimeric BAR protein Rvs (Rvs161/Rvs167) is implicated, although the scission mechanism remains unclear. We used quantitative live-cell imaging and genetic manipulation to understand the recruitment and function of Rvs and other potential scission effectors. We found that Rvs assembly is timed by interaction of its BAR domain with membrane curvature. A second domain, the SH3 domain, affects localization efficiency of Rvs. This SH3 dependent localization is mediated via myosin Myo3. Removal of the SH3 domain also affects actin assembly dynamics and invagination growth. Our results indicate that both BAR and SH3 domains are important for the role of Rvs in scission. We found that neither synaptojanins nor dynamin contribute directly to scission. We propose that the Rvs BAR domain stabilizes the membrane invagination, thereby delaying scission and allowing the invaginations to grow longer. We also propose that vesicle formation is dependent on the force exerted by the actin network component of the endocytic machinery.

## Introduction

Clathrin-mediated endocytosis is a process by which cargo molecules from the cell exterior are incorporated into a clathrin-coated vesicle that is then transported into the cell. Over 50 different proteins are involved in formation of an endocytic vesicle (*McMahon and Boucrot, 2011; Kaksonen and Roux, 2018*). The molecular mechanisms mediating endocytic vesicle formation are largely conserved between yeast and mammals. Most yeast endocytic proteins have homologues in mammals. These proteins establish endocytic sites, recruit cargo, bend the membrane into an invagination, and finally separate the endocytic vesicle from the plasma membrane (*Kaksonen and Roux, 2018*). Actin filaments have a critical role in membrane shaping in yeast. The filaments are nucleated and polymerize to form a branched actin network, which is required for bending the membrane into stereotypical tubular invaginations (*Kübler et al., 1993; Kukulski et al., 2012*). How the final stage of membrane scission is effected in yeast remains unclear. In mammalian cells, the forces that drive the final transition from invagination to spherical vesicle are largely provided by the GTPase dynamin (*Grigliatti et al., 1973; Sweitzer and Hinshaw, 1998; Ferguson et al., 2007; Takei et al., 1995; Galli et al., 2017*). Dynamin interacts via its proline-rich domain with the SH3 domains of crescent-shaped N-BAR proteins like Endophilin and Amphiphysin (*Grabs et al., 1997*;

39 **Cestra et al., 1999; Farsad et al., 2001; Ferguson et al., 2009; Meinecke et al., 2013**). Conformational  
40 changes of dynamin recruited to N-BAR molecules cause constriction of the underlying invaginated  
41 membrane, resulting in vesicle formation (**Shupliakov et al., 1997; Zhang and Hinshaw, 2001; Zhao**  
42 **et al., 2016**).

43 Three dynamin-like proteins: Dnm1, Mgm1, and Vps1, have been identified in yeast. Dnm1 and  
44 Mgm1 are involved in mitochondrial fusion and fission (**Cerney et al., 2007**). The third, Vps1, gets  
45 its name from its essential role in vacuolar protein sorting in the secretory pathway (**Rothman'**  
46 **et al., 1989; Rothman et al., 1990**). It is also involved in fission and fusion of vacuoles and perox-  
47 isomes (**Hoepfner et al., 2001; Peters et al., 2004**), and is required for regulation of endosome to  
48 Golgi trafficking (**Gurunathan et al., 2002**). In addition, Vps1 has been reported to localize at endo-  
49 cytic sites on the plasma membrane, interact with endocytic proteins like clathrin, and influence  
50 the lifetimes and recruitment of endocytic proteins (**Nannapaneni et al., 2010; Yu and Cai, 2004;**  
51 **Smaczynska-de Rooij et al., 2012**). Others however, have failed to observe Vps1 at endocytic sites  
52 (**Kishimoto et al., 2011; Goud Gadila et al., 2017**), or observe a role in endocytic vesicle scission  
53 (**Nothwehr et al., 1995; Kaksonen et al., 2005**). The role of Vps1 in clathrin-mediated endocytosis  
54 thus remains debated.

55 A confirmed component of the yeast endocytic scission mechanism is the heterodimeric complex  
56 formed by the N-BAR domain proteins Rvs161 and Rvs167 (**Munn et al., 1995; D'Hondt et al., 2000;**  
57 **Kaksonen et al., 2005; Kishimoto et al., 2011**). The two Rvs proteins are homologues of the N-BAR  
58 proteins Amphiphysin and Endophilin in animals (**Friesen et al., 2006; Youn et al., 2010**). Deletion  
59 of Rvs167 reduces scission efficiency by nearly 30% and reduces the lengths to which endocytic in-  
60 vaginations grow to nearly a third (**Kaksonen et al., 2005; Kukulski et al., 2012**). In endocytic events  
61 that fail to undergo scission, the membrane first invaginates and then retracts back to the plasma  
62 membrane (**Kaksonen et al., 2005**). Rvs167 and Rvs161 proteins form a canonical N-BAR domain  
63 which forms a crescent-shaped structure (**Youn et al., 2010**). This curved structure is thought to be  
64 the key functional domain of the protein (**Sivadon et al., 1997**). N-BAR domains are able to form lat-  
65 tices that can bind membrane with their concave surfaces, and impose or sense curvature across  
66 dimensions larger than that of a single BAR domain (**Farsad et al., 2001; Peter et al., 2004; Youn**  
67 **et al., 2010; Mim et al., 2012; Zhao et al., 2013**). In addition to the N-BAR domain, Rvs167 has a  
68 Glycine-Proline-Alanine rich (GPA) region and a C-terminal SH3 domain (**Sivadon et al., 1997**). The  
69 GPA region is thought to act as a linker with no other known function, while loss of the SH3 domain  
70 affects daughter cell budding and actin cytoskeleton morphology (**Sivadon et al., 1997**). The Rvs  
71 complex can tubulate liposomes in vitro, indicating that the BAR domain can impose curvature on  
72 membranes (**Youn et al., 2010**). However, Rvs arrives at endocytic sites when membrane tubes are  
73 already formed (**Kukulski et al., 2012; Picco et al., 2015**). Therefore curvature-sensing rather than  
74 curvature-generation is the likely role of the Rvs complex at endocytic sites. Rvs molecules arrive  
75 at endocytic sites a few seconds before scission, and disassemble rapidly just after scission (**Picco**  
76 **et al., 2015**), consistent with a role in vesicle scission. However, a mechanistic understanding of  
77 the role of Rvs in scission remains incomplete.

78 Synaptojanins are PI(4,5)P<sub>2</sub> phosphatases that have been implicated in endocytic scission, as well  
79 as in intracellular signalling, and modulation of the actin cytoskeleton (**Singer-Krüger et al., 1998**).  
80 They interact with both dynamin and N-BAR proteins in mammalian cells (**McPherson et al., 1996;**  
81 **Watanabe et al., 2018**). Disruption of these genes leads to accumulation of PIP<sub>2</sub> in cells (**Stolz et al.,**  
82 **1998b**). In synaptojanin deleted cells, coated endocytic vesicles cluster at the plasma membrane,  
83 demonstrating a role for lipid hydrolysis in vesicle uncoating (**Watanabe et al., 2018**). In yeast,  
84 removal of synaptojanin-like proteins affects rate of endocytosis, and induces aberrant behaviour  
85 of several endocytic proteins (**Singer-Krüger et al., 1998; Sun et al., 2007; Kishimoto et al., 2011**).

86 We aimed to identify roles and molecular mechanisms for proteins that have been implicated in the

87 scission of endocytic vesicles in yeast: Vps1, synaptojanins, and the Rvs complex. We used quan-  
88 titative live-cell imaging and genetic manipulation in *Saccharomyces cerevisiae* to test the roles of  
89 these proteins in endocytosis. We found evidence for a specific role in scission for the Rvs complex,  
90 but not for the other candidate proteins. Furthermore, we analyzed the molecular mechanisms of  
91 recruitment and the mode of action for Rvs in scission.

## 92 Results

### 93 **Rvs167, but not Vps1, influences endocytic coat internalization**

94 The role of the dynamin-like protein Vps1 in yeast endocytosis is unclear. Some studies have re-  
95 ported a role for Vps1 in endocytic vesicle scission (*Yu and Cai, 2004; Nannapaneni et al., 2010;*  
96 *Rooij et al., 2010*), while others have reported that Vps1 does not localize to endocytic sites or  
97 contribute to scission (*Kishimoto et al., 2011; Goud Gadila et al., 2017*). The question of whether  
98 or not Vps1 has a function at endocytic sites has been obfuscated by potential tagging-induced  
99 dysfunction of Vps1 molecules. Neither N- nor C-terminally tagged Vps1 co-localized with endo-  
100 cytic actin-binding protein Abp1 in our hands (data not shown), consistent with other work that  
101 observed localization only with the Golgi trafficking pathway (*Goud Gadila et al., 2017*).

102 In mammalian cells, dynamin interacts with N-BAR proteins to cause vesicle scission (*Grabs et al.,*  
103 *1997; Cestra et al., 1999; Farsad et al., 2001; Meinecke et al., 2013*). Although the association  
104 between yeast dynamin Vps1 and N-BAR protein Rvs is uncertain, Rvs is recruited to endocytic sites  
105 briefly before scission and influences scission efficiency (*Kaksonen et al., 2003, 2005; Kukulski et al.,*  
106 *2012; Picco et al., 2015*). In order to determine the roles of these proteins in endocytic scission, we  
107 analyzed the behaviour of other endocytic proteins in cells lacking Vps1 and Rvs167, and compared  
108 against wild-type (WT) cells (Fig.1A-F).

109 Vps1 gene deletion was confirmed by sequencing the gene locus. *vps1Δ* cells showed a previously  
110 reported slow growth phenotype at high temperatures (Fig.S1A, *Rothman and Stevens (1986)*). In  
111 order to quantify invagination progression, coat protein Sla1 tagged at the C-terminus with eGFP  
112 was observed in yeast cells imaged at the equatorial plane (Fig.1A). Since membrane invagination  
113 progresses perpendicularly to the plane of the plasma membrane, proteins that move into the  
114 cytoplasm during invagination growth do so in the imaging plane. Upon actin polymerization, the  
115 endocytic coat moves into the cytoplasm along with the membrane as it invaginates (*Skruzny et al.,*  
116 *2012*). Movement of Sla1 thus acts as a proxy for the growth of the plasma membrane invagina-  
117 tion. Membrane retraction, that is, inward movement and subsequent retraction of the invaginated  
118 membrane back towards the cell wall is a scission-specific phenotype (*Kaksonen et al., 2005; Kishi-*  
119 *moto et al., 2011*). Retraction rates were not significantly different in *vps1Δ* cells compared to the  
120 WT (Fig.1B).

121 To follow invaginations in more detail, centroid trajectories of 30-50 Sla1-eGFP patches in *vps1Δ*  
122 and WT cells were tracked and compared (Fig.1A-C). Centroids of Sla1 patches- each patch being  
123 an endocytic site- were tracked in time and averaged. This provided an averaged centroid that  
124 could be followed with high spatial and temporal precision (*Picco et al., 2015*). The movement of  
125 the Sla1-eGFP centroid corresponds to the growth of the endocytic membrane invagination and to  
126 the initial diffusive movement of the vesicle after scission (*Kukulski et al., 2012; Picco et al., 2015*).  
127 The distance that Sla1 centroid moves thus gives an indication of invagination and scission steps of  
128 endocytosis. Any defects in scission are expected to change the motility pattern of the Sla1 centroid.

129 The movement of Sla1-eGFP in WT cells was linear to about 150 nm (Fig.1C), consonant with maxi-  
130 mum invagination lengths measured by correlative light and electron microscopy (CLEM) (*Kukulski*

**131** *et al., 2012)*. Sla1 movement in *vps1Δ* cells was virtually identical to WT cells (Fig.1C). The total  
**132** movement- and so the length of endocytic invagination - was similar to WT.

**133** Quantitative imaging has shown that scission is simultaneous with a sharp jump of the Rvs167  
**134** centroid into the cytoplasm and a corresponding loss of fluorescent intensity (Fig.1 D,F, S1B) (*Picco*  
**135** *et al., 2015; Kukulski et al., 2012*). This jump is interpreted as loss of protein on the membrane  
**136** tube at the time of scission, causing an apparent jump of the centroid to proteins that remain  
**137** localized on the newly formed vesicle. Kymographs of Rvs167-GFP (Fig.1A), as well as Rvs167 cen-  
**138** troid tracking (Fig.1F) in *vps1Δ* cells showed the same jump as in WT. We quantified the number of  
**139** molecules of Rvs167 recruited to endocytic sites in *vps1Δ* cells (*Picco et al., 2015; Joglekar et al.,*  
**140** *2006*), and found that it was not significantly different from that recruited to WT cells (Fig.1D). We  
**141** expect that a longer invagination is likely to recruit either more molecules of Rvs167 or the same  
**142** number of molecules distributed along a longer invagination. Since we observe neither higher  
**143** molecules numbers, nor larger invagination lengths, we conclude that the membrane tube is the  
**144** same length as in WT. These data further suggest that the scission process is normal in *vps1Δ* cells.

**145** We next studied invagination progression in cells lacking Rvs167. Since the Rvs complex is a dimer  
**146** of Rvs161 and Rvs167 (*Boeke et al., 2014*), deletion of RVS167 gene effectively removes both pro-  
**147** teins from endocytic sites (*Lombardi and Riezman, 2001; Kaksonen et al., 2005*). We quantified  
**148** the effect of *rvs167Δ* on membrane invagination (Fig.1A,B,E). When Sla1 was observed in *rvs167Δ*  
**149** cells, nearly 30% of endocytic events displayed the beginning of movement away from the starting  
**150** position- thus invagination formation- then retract back to starting position (Fig.1A). Retractions  
**151** indicate failure of vesicle formation. Thus only about 70% of Sla1 patches underwent apparently  
**152** successful scission in *rvs167Δ* cells (Fig.1B). Similar scission rates have been measured in earlier  
**153** studies (*Kaksonen et al., 2005; Rooij et al., 2010; Kishimoto et al., 2011*). We classified endocytic  
**154** events into successful and retracting events and analyzed the average centroid movement in these  
**155** two classes. Sla1 centroid movement in both successful and retracting endocytic events in *rvs167Δ*  
**156** cells look similar to WT up to invagination length of about 50 nm (Fig.1E). In WT cells, Abp1 intensity  
**157** begins to drop at scission time (Fig.S1B, *Picco et al. (2015)*). Abp1 intensity in *rvs167Δ* cells dropped  
**158** after Sla1 centroid moved about 50 nm, suggesting that scission occurs in successful events at  
**159** invagination lengths around 50 nm (Fig.S1D). That membrane scission occurs at shorter invagina-  
**160** tion lengths than in WT is corroborated by the smaller vesicles found using CLEM in *rvs167Δ* cells  
**161** (*Kukulski et al., 2012*). CLEM has moreover shown that Rvs167 localizes to endocytic sites after the  
**162** invaginations are about 50 nm long (*Kukulski et al., 2012*). Normal initial Sla1 movement in *rvs167Δ*  
**163** indicates therefore that membrane invagination is unaffected till Rvs would normally arrive.

#### **164** **Synaptojanins influence vesicle uncoating, but not scission dynamics.**

**165** As Vps1 did not appear to influence membrane scission, we proceeded to test the potential role  
**166** of synaptojanins in scission (*Liu et al., 2009*). Apart from their role in vesicle uncoating, synapto-  
**167** janins have been proposed to mediate scission with their PI(4,5)P<sub>2</sub> hydrolysis activity (*Sun et al.,*  
**168** *2007; Toret et al., 2008*). In this model, BAR domains coat the invaginated tube, and preferential  
**169** hydrolysis of PIP<sub>2</sub> at the invagination tip unprotected by BAR proteins generates line tension, even-  
**170** tually causing membrane scission. We reasoned that if the yeast synaptojanins are involved in  
**171** scission, their deletion should alter the invagination dynamics visualized with Sla1-eGFP or Rvs167-  
**172** eGFP. Three synaptojanin-like proteins have been identified in *S. cerevisiae*: Inp51, Inp52, and Inp53.  
**173** Inp51-eGFP exhibits a diffuse cytoplasmic signal, Inp52-eGFP localizes to endocytic sites, and Inp53  
**174** localizes to patches within the cytoplasm (Fig.2A) (*Bensen et al., 2000; Sun et al., 2007*). Since Inp52  
**175** can be observed at endocytic sites, we began with determining the spatial and temporal recruit-  
**176** ment of Inp52 within the endocytic machinery. We tracked and aligned the averaged centroid of  
**177** Inp52 spatially and temporally in relation to other endocytic proteins. In order to do this, we im-

178 aged Inp52-eGFP simultaneously with Abp1-mCherry. We also imaged Sla1-eGFP and Rvs167-eGFP  
179 together with Abp1-mCherry. Using Abp1 as the common reference frame, we were able to com-  
180 pare the arrival of the different proteins with respect to that of Abp1. We assigned as time =0 s,  
181 the peak fluorescent intensity of Abp1. In WT cells, this peak is concomitant with membrane scis-  
182 sion, and also coincides with the peak Rvs167 fluorescent intensity (S1B, *Picco et al. (2015)*). On  
183 the y-axis, 0 nm indicates the non-motile position of the Sla1 centroid. Positions of the other cen-  
184 troids are spatially and temporally aligned to each other (Fig.2B). This analysis showed that Inp52  
185 molecules arrived after Rvs167, and localized to the invagination tip. The localization and assembly  
186 dynamics of Inp52 are consistent with a role in the late stage of membrane invagination.

187 Inp53 was not investigated further because it could not be detected at endocytic sites (Fig.2A), and  
188 is likely localized to the trans-Golgi network (*Bensen et al., 2000*). Although we were unable to  
189 observe localization of Inp51 at the plasma membrane (Fig.2A), deletion of Inp51 has been shown  
190 to exacerbate the effect of *inp52Δ* on endocytosis (*Singer-Krüger et al., 1998*), so both Inp51 and  
191 Inp52 were tested as potential scission regulators.

192 *inp51Δinp52Δ* cells have dramatic morphological and growth defects, defects in vacuole morphol-  
193 ogy and budding polarity (*Singer-Krüger et al., 1998; Stolz et al., 1998a*). These cells also have  
194 drastically altered PIP<sub>2</sub> levels (*Stolz et al., 1998b*), which likely affect the assembly, disassembly, and  
195 function of many PIP<sub>2</sub>-binding endocytic proteins. The double mutation reportedly causes aberra-  
196 tions in endocytic coat, myosin, and actin network behaviour (*Sun et al., 2007*). Coat proteins Sla1,  
197 Sla2 and Ent1 have elongated lifetimes at endocytic sites, as does type I myosin Myo5, and Rvs167.  
198 Time taken for Abp1 assembly and disassembly is more than doubled (*Sun et al., 2007*). That mul-  
199 tiple endocytic phases, including scission, are affected in the double mutation makes it difficult to  
200 demonstrate a direct role in scission. Patches of Rvs167-eGFP tracked in these cells persist instead  
201 of disassembly immediately after inward movement, leading to aggregation of fluorescent patches  
202 inside the cytoplasm (Fig.S2B). We cannot, by the methods used here, distinguish between scission  
203 and other defects. We reasoned that a quantitative analysis of single mutants was therefore bet-  
204 ter suited to reveal a scission-specific function for synaptojanins, without perturbing overall PIP<sub>2</sub>  
205 homeostasis.

206 Dynamics of Sla1-eGFP and Rvs167-eGFP in *inp51Δ* and *inp52Δ* cells were compared against the  
207 WT (Fig.2C-E). Scission efficiency did not significantly decrease in *inp51Δ* compared to the WT, but  
208 showed a slight decrease in *inp52Δ* cells (Fig.2C). The movement of Sla1 and Rvs167 centroids in  
209 successful endocytic events in *inp51Δ* were virtually the same as in WT (Fig.2 D,E), while Rvs167  
210 assembly and disassembly took longer (Fig.S2A). Rvs167 signal in *inp51Δ* cells persisted longer  
211 compared to the WT (Fig.2E), likely because of a delay in Rvs167 disassembly from the newly formed  
212 vesicle. In *inp52Δ* cells, Sla1 movement had the same magnitude and rate as in WT, but Sla1-eGFP  
213 signal was persistent after inward movement (Fig.2D). Sla1 assembly and disassembly was aberrant  
214 in *inp52Δ* cells compared to WT (Fig.S2A). These data are consistent with synaptojanin involvement  
215 in assembly and disassembly of coat and scission proteins at endocytic sites (*Toret et al., 2008*).  
216 However, because the centroid movements of Sla1 and Rvs167 are unaltered, synaptojanins may  
217 not have a direct or major role in membrane scission.

## 218 **Rvs BAR domains recognize membrane curvature in vivo**

219 So far Rvs167 and Rvs161 remain the proteins that have the most significant influence on scission  
220 efficiency. Recruitment to and interaction of the Rvs complex at endocytic sites was thus investi-  
221 gated further. The Rvs complex can tubulate liposomes in vitro, likely via the BAR domain (*Youn  
222 et al., 2010*). Interaction of the BAR domain with membrane curvature in vivo has however not  
223 been tested. The Rvs167-SH3 domain can interact with proteins associated with actin patches

such as Abp1, Las17, Myo3, Myo5 and Vrp1, but the role of these interactions in vivo is not known (*Lila and Drubin, 1997; Colwill et al., 1999; Madania et al., 1999; Liu et al., 2009*). We first tested the BAR-membrane interaction by deleting the SH3 domain to remove its contribution (Fig.3A). We then observed localization of Rvs167-sh3Δ in *sla2Δ* cells, which do not have membrane curvature at endocytic sites (*Picco et al., 2018*). Sla2 acts as the molecular linker between forces exerted by the actin network and the plasma membrane (*Skruzny et al., 2012*). *sla2Δ* cells therefore contain a polymerizing actin network at endocytic patches, but the membrane has no curvature, and endocytosis fails (*Skruzny et al., 2012; Picco et al., 2018*). Colocalization of endogenously tagged full-length Rvs167-eGFP and Rvs167-sh3Δ-eGFP with Abp1-mCherry in WT and *sla2Δ* cells were compared (Fig.3B). We thus tested whether Rvs BAR domain could be recruited to the endocytic sites in *sla2Δ* independent of membrane curvature. In *sla2Δ* cells, the full-length Rvs167 co-localized with Abp1-mCherry indicating that it was recruited to endocytic sites without membrane curvature (Fig.3B, "*sla2Δ*"). Rvs167-sh3Δ did not appear at the plasma membrane except for rare transient patches. Therefore, Rvs167-sh3Δ, that is, the BAR domain alone, is not recruited to endocytic sites in the absence of curvature in *sla2Δ* cells. Localization of the full-length protein in *sla2Δ* cells is therefore likely via SH3 domain interaction.

#### 240 **Rvs SH3 domains have an actin and curvature-independent localisation**

241 We wanted to distinguish between Rvs association with membrane curvature and actin. Latrunculin A (LatA) inhibits actin polymerization, and therefore the assembly of actin and actin related proteins at endocytic sites. *sla2Δ* as well as LatA remove membrane curvature, but *sla2Δ* retains actin patches at endocytic sites (*Kukulski et al., 2012; Picco et al., 2018*). To study the interaction of Rvs at endocytic sites without actin proteins, we observed the localization of Rvs167 and Rvs167-sh3Δ in LatA treated WT cells (Fig.3B, "LatA"). We also observed full-length and mutant protein in *sla2Δ* cells treated with LatA, so that we could be sure that we removed any capacity for membrane curvature, as well as actin related proteins (Fig.3B, "*sla2Δ* + LatA"). Full-length Rvs167 localized transiently at the plasma membrane in WT cells treated with LatA as well as in *sla2Δ* cells treated with LatA (Fig.3B). Rvs167-sh3Δ did not localize to the plasma membrane in either case. Thus, localization of full-length Rvs167 in the presence of LatA in WT and *sla2Δ* cells is due to the SH3 domain. This also indicates that the SH3 domain is able to recruit Rvs molecules to the plasma membrane in an actin- and curvature-independent manner.

#### 254 **Rvs167 SH3 domains are likely recruited by Myo3**

255 Type I myosins Myo3 and Myo5, and yeast verprolin Vrp1 have known genetic or physical interactions with the Rvs167 SH3 domain (*Lila and Drubin, 1997; Colwill et al., 1999; Madania et al., 1999; Liu et al., 2009*). We tested the possible role of these proteins in the SH3 domain dependent localization of Rvs167 in cells with the gene for one of these proteins deleted, and treated with LatA (Fig.4). By using LatA we expected to reproduce the situation in which the interaction between the BAR domain and curved membrane is removed. Then, if we lost SH3 interaction because we removed the protein with which it interacts, we would lose localization of Rvs167 completely. Neither Vrp1 nor Myo5 deletion in combination with LatA treatment removed the localization of Rvs167: 88% and 87% cells respectively still showed Rvs167 localization, similar to WT localization. Deletion of Myo3 with LatA treatment reduced localization of Rvs167 (43.4% of cells with localization), indicating that SH3 domains interact at endocytic sites primarily with Myo3.

**266    Deletion of Rvs167 SH3 domain affects coat and actin dynamics**

267    Since the Rvs167-SH3 domain had an influence on the recruitment of the Rvs complex to endocytic  
268    sites, we wondered if the domain affects not just recruitment of the protein, but also invagination  
269    progression. We compared dynamics of coat, actin, and scission markers in WT and *rvs167-sh3Δ*  
270    cells (Fig.5).

271    The maximum Sla1 centroid movement in *rvs167-sh3Δ* cells is 50-70 nm compared to about 150 nm  
272    in WT, and takes about 10 s compared to about 6 s in WT (Fig.5A,B). The total movement of Rvs167-  
273    sh3Δ centroid is half that of full-length Rvs167 (Fig.5A,B). Reduced movements of both Sla1 and  
274    Rvs167-sh3Δ centroids in *rvs167-sh3Δ* cells are consistent with the formation of shorter endocytic  
275    invaginations in these cells.

276    We observed a delay in Rvs167-sh3Δ recruitment compared to the onset of Abp1 recruitment  
277    in *rvs167-sh3Δ* cells compared to WT (Fig.5 C,D). In WT cells, the number of Rvs167 and Abp1  
278    molecules peak at the same time. Thus, the actin network begins disassembling as soon as scis-  
279    sion occurs (Fig.5C). However, in *rvs167-sh3Δ* cells, the numbers of Rvs167 and Abp1 molecules  
280    peaked asynchronously, with Rvs167 peaking later. This observation suggests that there is a feed-  
281    back mechanism between the actin network and membrane scission, and that this feedback is  
282    disrupted in *rvs167-sh3Δ* cells. Rvs167-sh3Δ accumulation began when Abp1 molecule number in  
283    the mutant was the same as in WT (about 300 copies, Fig.5C,D). Both Rvs167 and Rvs167-sh3Δ  
284    molecules arrived at endocytic sites when the Sla1 centroid was 20-30 nm away from its starting  
285    position: so the endocytic coat has moved at least 20 nm when both WT and mutant forms of Rvs  
286    start to be recruited. That Rvs167-sh3Δ recruitment begins at a certain length of the invagination  
287    suggests that the Rvs complex is recruited to a specific geometry of membrane invagination. Then  
288    Rvs167-sh3Δ accumulation is delayed because invaginations in these cells take longer to acquire  
289    this geometry. We think that Rvs molecules in WT cells may arrive below our detection threshold,  
290    and that the arrival of the molecules supports invagination growth. As the invagination grows, Rvs  
291    continues to accumulate on the invagination tubes, and molecule numbers are eventually large  
292    enough to be detected. In support of this, CLEM has shown that when Rvs167 molecules are de-  
293    tected at endocytic sites, the invaginations are about 60 nm long, shortly after the membrane  
294    is already tubular (*Picco et al., 2015; Kukulski et al., 2012*). Since Rvs167-sh3Δ molecules accu-  
295    mulate slower than full-length protein, their support to membrane growth is less effective, and  
296    the invagination grows slower. Abp1 accumulation correlates with invagination growth, so slower  
297    invagination growth accumulates Abp1 slower. Recruitment of Rvs167-sh3Δ was significantly re-  
298    duced compared to Rvs167 (Fig.5C,D), although cytoplasmic concentration of both were similar  
299    (Fig.S4). Recruitment therefore is unlikely to be limited by expression of the mutant protein. Abp1  
300    disassembly time was increased to 15 s in *rvs167-sh3Δ* cells compared to 5 s in WT, and number of  
301    Abp1 molecules recruited was reduced from 600 to about 400, 60% of WT recruitment (Fig.5C,D).  
302    Recruitment and disassembly defects of Abp1 indicate disruption of actin network dynamics in  
303    *rvs167-sh3Δ* cells.

**304    Increased BAR domain recruitment corresponds to increased membrane movement**

305    Reduced Sla1 movement was observed in both *rvs167Δ* (Fig.1) and *rvs167-sh3Δ* (Fig.5) cells, in which  
306    about half the WT number of Rvs167 molecules are recruited (Fig.5). This suggests that increased  
307    Sla1 movement correlates with increased recruitment of Rvs167. We wondered if Sla1 movement  
308    would scale with amount of Rvs recruited to endocytic sites. This could suggest that recruitment of  
309    Rvs BAR domains scaffolds the membrane invagination and protects it against membrane scission  
310    (*Boucrot et al., 2012; Dmitrieff and Nédélec, 2015*). We titrated the amount of Rvs expressed in  
311    cells by duplicating the open reading frame of RVS167 and RVS161 genes (*Huber et al., 2014*). We

312 also generated a strain in which the *rvs167-sh3Δ* gene was duplicated . We thus obtained cells  
313 containing either 2x copies of both RVS genes (2xRVS), 1x copy of the RVS genes (1xRVS, ie WT), 2x  
314 copies of *rvs167-sh3Δ* (2xBAR), or 1x copy of *rvs167-sh3Δ* (1xBAR) (Fig.6A-D). In the 2xBAR strain,  
315 RVS161 was not duplicated. This is because we measured the number of molecules of mutant  
316 *Rvs167* recruited in the 2xBAR strain with and without RVS161 duplicated, and found that they were  
317 the same, suggesting that *Rvs161* protein expression is not limiting for assembly of the *Rvs* complex  
318 (data not shown). So we used the genetically simpler strain, without the RVS161 duplication.

319 Maximum number of WT and mutant *Rvs167* molecules recruited at endocytic sites varied in 1xRVS  
320 (WT), 2xRVS, 1xBAR, 2xBAR strains between 50 and 180 copies (Fig.6A, S6). Excess *Rvs* recruited in  
321 2xRVS cells (compared to 1xRVS) did not change the total movement of *Rvs167*, but *Rvs* disassem-  
322 bly takes longer (Fig.6A,B). In the 2xBAR case, amount of *Rvs167-sh3Δ* molecules recruited to en-  
323 docytic sites increased compared to 1xBAR, as did the movement of the centroid (Fig.6A, B). BAR  
324 domain recruitment increased from 1xBAR, to 2xBAR, 1xRVS, and was finally maximal in 2xRVS  
325 cells. The trend of inward movement of the *Rvs167* centroid suggests that movement correlates  
326 with number of BAR molecules recruited to sites, but saturates in the case of 2xRVS. The delayed  
327 disassembly compared to 1xRVS may be due to a change in interaction between the BAR domains  
328 and underlying membrane. The membrane may be already saturated with bound RVS, causing  
329 perhaps interaction between *Rvs* dimers rather than *Rvs* and membrane. Alternatively, excess *Rvs*  
330 molecules may be recruited to the vesicle, so there is a delay in disassembly of these molecules  
331 compared to those on the invagination tube.

332 *Abp1* molecule numbers and lifetimes at endocytic sites were different between the 1xRVS 2xRVS,  
333 1xBAR, 2xBAR strains (Fig.6D, S5). Total *Abp1* molecules recruited were reduced in 1xBAR com-  
334 pared to the 2xBAR, 1xRVS and 2xRVS (Fig.6D, Fig.S6). As *Abp1* molecule numbers increased,  
335 shorter lifetimes, approaching that of WT *Abp1* were observed (Fig.S5). Comparing between the  
336 1xRVS (WT), 2xRVS, 1xBAR, 2xBAR strains, the cells with higher *Abp1* molecule numbers showed  
337 larger total movement of the *Sla1* centroid (Fig.6C,D). This indicates a correlation between the  
338 maximum number of *Abp1* molecules recruited and total invagination length. In *rvs167Δ* cells,  
339 measured *Abp1* molecule numbers were about the same as in WT (Fig.6D). Quantification of *Abp1*  
340 molecule numbers in these cells is confounded by the existence of two types of endocytic events:  
341 successful and retracting events. We were unable to separate these events in the molecule number  
342 quantification, but we speculate that retracting events may continue to assemble an actin network  
343 after or during retraction. This accumulation could compensate for smaller *Abp1* numbers that  
344 may have been measured at successful endocytic events. A much smaller percentage of endocytic  
345 events in 1BAR and 2xBAR retract, so we do not expect retracting endocytic invaginations in these  
346 cells to confound the *Abp1* quantification significantly (Fig.S6).

347 We found that increasing the expression of RVS caused increased recruitment of *Rvs* molecules  
348 to endocytic sites. We also found that the number of *Rvs* BAR domains recruited to membrane  
349 invaginations correlates positively with total length of the invagination. Furthermore, this length  
350 of the invagination also correlates positively with the number of *Abp1* molecules recruited.

## 351 Discussion

352 Recruitment and function of the *Rvs* complex has been studied in this work, and the applicability  
353 of several membrane scission models to yeast endocytosis have been tested. We propose that *Rvs*  
354 is recruited to endocytic sites via interactions between the BAR domains and invaginated mem-  
355 brane, and also via SH3 mediated protein-protein interactions. SH3 interactions are required for  
356 efficient recruitment of *Rvs*. We found that assembly of *Rvs* at the membrane invagination delays  
357 membrane scission, allowing the invagination to grow to its full length. WT invagination growth de-

358 depends on recruitment of a critical number of Rvs molecules. Both timing and recruitment efficiency  
359 of Rvs appear crucial to Rvs function.

### 360 **BAR domains sense in vivo membrane curvature and time the recruitment of Rvs**

361 The curved structure of Endophilin and Amphiphysin BAR domains allows them to interact with  
362 curved membranes. These proteins are able to form organized assemblies on tubular membranes  
363 in vitro (*Mim et al., 2012*). Rvs167-sh3Δ localized to endocytic sites when curvature was present  
364 (Fig.3B, "Untreated"). Without the SH3 domain, and in the absence of membrane curvature in *sla2Δ*  
365 cells, Rvs167-sh3Δ did not localize to endocytic sites (Fig.3, "*sla2Δ*"). This indicates that the Rvs167-  
366 sh3Δ localization was via BAR-membrane curvature interaction. This demonstrates that the Rvs  
367 BAR domain senses and requires membrane curvature to interact with endocytic sites. Rvs167-  
368 sh3Δ had a similar average lifetime at endocytic sites as full-length Rvs167 (Fig.5A,B). However, time  
369 alignment with Abp1 showed that there was a delay in the recruitment of Rvs167-sh3Δ (Fig.5C,D).  
370 Sla1 centroid movement was slower in *rvs167-sh3Δ* cells than in WT cells. So it takes longer for the  
371 membrane in these cells to reach the same invagination length as WT. We propose that the start  
372 of Rvs recruitment is timed to a specific membrane invagination length - therefore to a specific  
373 membrane curvature - accounting for the delay in recruitment of Rvs167-sh3Δ. The precise timing  
374 of recruitment is therefore provided by the BAR domain interacting with membrane at a specific  
375 curvature.

### 376 **SH3 domains allow efficient and actin- and membrane curvature- independent re- 377**ruitment of Rvs

378 Rvs167-sh3Δ accumulated to about half the number of full length Rvs167 (Fig.5C,D) even though  
379 similar cytoplasmic concentration was measured for both proteins (Fig.S4), indicating that loss of  
380 the SH3 domain decreases the efficiency of recruitment of Rvs to endocytic sites. In *sla2Δ* cells, full-  
381 length Rvs167 forms patches on the membrane (Fig.3B, "*sla2Δ*"). Since Rvs167-sh3Δ does not local-  
382 ize to the plasma membrane in *sla2Δ* cells, localization of the full-length protein must be mediated  
383 by the SH3 domain. The full-length Rvs167 is able to assemble and disassemble at cortical patches  
384 in *sla2Δ* cells, that is, without the curvature-dependent interaction of the BAR domain (Fig.S3). This  
385 indicates recruitment and disassembly of Rvs can occur via interactions between its SH3 domains  
386 and endocytic sites. In *sla2Δ* cells treated with LatA (Fig.3B, "*sla2Δ+ LatA*"), both membrane cur-  
387 vature and actin are removed from endocytic sites. Full-length Rvs167 in these cells still shows  
388 transient localizations at the plasma membrane. Therefore the SH3 domain is able to localise the  
389 Rvs complex in an actin- and curvature- independent manner.

### 390 **Recruitment of Rvs167 affects endocytic actin network dynamics**

391 In WT cells, the Abp1 and Rvs167 fluorescent intensities peaked concomitantly (Fig.5C,D), and the  
392 consequent decay of both coincided. Membrane scission occurs around the intensity peak of  
393 Rvs167 (*Kukulski et al., 2012; Picco et al., 2015*). Coincident disassembly therefore indicates that  
394 upon vesicle scission, the actin network is rapidly disassembled. This coincident peak was lost  
395 in *rvs167-sh3Δ* cells: Rvs167-sh3Δ fluorescent intensity peaks a few seconds after Abp1 intensity  
396 starts to drop. The decay of Abp1 is also prolonged, taking over double the time as in WT. Although  
397 it is not clear what the decoupling of Abp1 and Rvs167-sh3Δ peaks means, the changes in Abp1  
398 dynamics suggests a strong disruption of the actin network. In 1xBAR cells, the average lifetime of  
399 actin marker Abp1 was about 25 s (Fig.S5). This lifetime decreases in 2xBAR cells to about 20 s, a  
400 shift towards the WT Abp1 lifetime of around 10 s. Therefore we conclude that recruitment of the  
401 Rvs BAR domains to the invagination regulates actin network dynamics.

402 **Rvs acts as a membrane scaffold, delaying membrane scission**

403 Final invagination length in non-retracting endocytic events in *rvs167Δ* cells was about 50 nm  
404 (Fig.1E), only a third the WT length. Together with electron microscopy data (*Kukulski et al., 2012*),  
405 this shows that scission can occur at much shorter invagination lengths. In WT cells, scission does  
406 not occur at these lengths, instead invaginations grow to 150 nm (*Kukulski et al., 2012*). Since  
407 invagination lengths were increased, compared to *rvs167Δ* and 1xBAR, by overexpression of the  
408 Rvs167-sh3Δ protein, that is, in 2xBAR (Fig.6A,C), we think that localization of Rvs-BAR domains to  
409 the membrane tube stabilizes the membrane (*Boucrot et al., 2012; Dmitrieff and Nédélec, 2015*)  
410 and allows invaginations to progress. Yeast endocytosis is heavily dependent on a dynamic actin  
411 network to generate the forces that sever the membrane (*Kübler et al., 1993; Kaksonen et al.,  
412 2003; Picco et al., 2018*). We propose that Rvs accumulation stabilizes the membrane invagination  
413 and thereby also increases the amount of actin required to sever the membrane. This allows the  
414 invagination to grow until WT invagination length is reached. We speculate that continued invagina-  
415 tion growth allows the actin network to generate enough force to compensate for the stabilization.  
416 There is a limit to the stabilization by BAR domains: in 2xRVS cells, invagination lengths are the  
417 same as in 1xRVS cells even though more Rvs is recruited. It is possible that the nature of the Rvs  
418 complex interaction with the membrane changes after a certain amount of Rvs is recruited. Once  
419 the membrane is saturated with Rvs molecules, BAR domains may interact with each other rather  
420 than with the underlying membrane. This could explain the changes in the disassembly dynamics  
421 of Rvs in the 2xRVS case (Fig.6A).

422 If enough forces are generated at around 50 nm, why is scission inefficient and membrane retrac-  
423 tion rates increased in *rvs167Δ* compared to WT? Forces generated by the actin network may be  
424 at a threshold level when the invaginations are short. There could be enough force to sever the  
425 membrane, but not enough to sever reliably. The Rvs scaffold may then stabilize the membrane  
426 invagination, preventing retraction, and allowing it to continue growing. This subsequently allows  
427 the actin network to continue growing, accumulating actin. Eventually enough actin is accumu-  
428 lated to reliably cause scission. We hypothesise that increased actin amount yields higher force on  
429 the membrane. This force stretches the membrane, eventually breaking it. Controlling membrane  
430 tube length could also be a way for the cell to control the size of the vesicles formed, and therefore  
431 the amount of cargo that can be packed into the vesicle.

432 **What causes membrane scission?**

433 We have tested candidate proteins implicated in yeast endocytic scission and looked for scision  
434 defects. Increased Sla1 retraction rates would indicate higher rate of scission failure. Larger total  
435 movement of Sla1 and Rvs167 centroids would indicate that a longer invagination has been formed,  
436 and that scission has not occurred at normal invagination lengths. We did not see longer centroid  
437 movement of Sla1 or Rvs167 in any mutants that we studied other than in Rvs mutants. In *vps1Δ*  
438 cells, there is no major change in retraction rate, nor are there changes in Sla1 or Rvs167 dynamics.  
439 We conclude that Vps1 is not necessary for Rvs localization or function, and is not necessary for  
440 scission.

441 Sla1 and Rvs167 centroid dynamics showed that deletion of either Inp51 or Inp52 resulted in  
442 scission delay. In *inp51Δ* cells, Rvs167 assembly was slightly slower than that in WT: Inp51 could  
443 play a role in Rvs recruitment. In the *inp52Δ* cells, about 12% of Sla1-GFP tracks retracted. Inp52  
444 has a moderate influence on scission efficiency, but this is not reflected in our observation of in-  
445 vagination dynamics. Rvs167 centroid persisted after scission in *inp52Δ* cells, so disassembly of  
446 Rvs after scission was delayed. Sla1 signal also persists for longer after scission in *inp52Δ* than  
447 in WT cells, suggesting that post-scission disassembly of coat proteins from the vesicle is inhib-

448 ited in *inp52Δ* cells. Inp52 likely plays a role in recycling endocytic proteins from the vesicle to  
449 the cytosolic pool. Synaptojanins may help recruit Rvs at endocytic sites: Inp51 and Inp52 have  
450 proline rich regions that could act as binding sites for Rvs167 SH3 domains. They are involved in  
451 vesicle uncoating post-scission, likely by dephosphorylating PIP<sub>2</sub> and inducing disassembly of PIP<sub>2</sub>  
452 -binding endocytic proteins. The synaptojanins do not appear to play a major role in scission, but  
453 Inp51 and Inp52 may function synergistically to influence membrane tension. The compounded  
454 problems related to lipid hydrolysis, and lack of tools that have the time resolution to measure the  
455 membrane tension *in vivo* prevent us from conclusively ruling out line tension as contributor to  
456 yeast endocytic scission.

457 Our RVS duplication data is able to test whether the protein friction model is applicable to yeast  
458 endocytic scission (*Simunovic et al., 2017*). According to this model, a frictional force between a  
459 moving membrane tube and a coat of BAR protein bound to it causes the tube to undergo scission.  
460 Therefore, a higher frictional force should break the tube faster than a lower force. We increased  
461 the frictional force on the membrane by increasing the number of BAR domains bound to the mem-  
462 brane tube, in 2xRVS cells. In 2xRVS cells, adding up to 1.6x the WT amount of Rvs at faster rates  
463 to membrane tubes did not affect the length at which the membrane undergoes scission (Fig.6).  
464 In *rvs167Δ* cells, frictional forces generated should be reduced compared to WT cells. Rather than  
465 increased Sla1 movement as this model would predict, we observed decreased Sla1 movement  
466 (Fig.1). We therefore think that protein friction does not contribute significantly to membrane scis-  
467 sion in yeast endocytosis.

468 A similar amount of Abp1 is recruited in both 1xRVS and 2xRVS cases, corresponding to coat move-  
469 ment of about 150 nm. Magnitude of coat movement correlates with the total amount of Abp1, and  
470 therefore, with the amount of actin recruited. A dynamic actin network is required for endocytosis  
471 in yeast (*Kübler et al., 1993; Picco et al., 2018*), and such a network is able to generate force (*The-  
472 riot et al., 1992*). Coupling between the actin network and membrane is necessary for invagination  
473 formation (*Skruzny et al., 2012; Picco et al., 2018*). The current understanding of yeast endocyto-  
474 sis suggests that the membrane is pushed into the cytoplasm by an actin network polymerizing  
475 at the base of the invagination, that is mechanically coupled to the invagination tip. More actin  
476 recruitment can generate higher force (*Bieling et al., 2016*). Actin may also provide a scaffold that  
477 aids membrane invagination. More actin is therefore consistent with scaffolding as well as with in-  
478 creased force generation. We propose that increased Abp1 recruitment - and therefore increased  
479 actin - leads to an increasing pushing force on the membrane, and that this force is responsible for  
480 invagination growth as well as for membrane scission. Stretching the membrane may eventually  
481 cause it to break, causing vesicle formation. The amount of force necessary to break the membrane  
482 is determined by properties of the membrane like rigidity and tension, properties of the proteins  
483 accumulated on the membrane, and by the high intracellular turgor pressure in yeast cells (*Dmitri-  
484 eff and Nédélec, 2015*). Once this force is overcome, vesicle scission occurs, and membrane-bound  
485 Rvs is released. Release of Rvs could cause instabilities in membrane shape that could also lead  
486 to scission (*Dmitrieff and Nédélec, 2015*). It is unclear whether scission causes release of Rvs, or  
487 vice-versa. The observation that Rvs167 can accumulate and disassemble on the membrane in the  
488 absence of membrane curvature (in *sla2Δ* cells) suggests that binding-unbinding can be mediated  
489 by another interaction partner. This allows us to speculate that Rvs release can be triggered by  
490 this partner. A method for detection scission with high temporal resolution is needed to resolve  
491 whether Rvs release of scission occurs first. Release of the SH3 domains could indicate to the actin  
492 network that vesicle scission has occurred, influencing disassembly of actin components.

493 We propose that Rvs is recruited to endocytic sites by two distinct mechanisms. SH3 domain of  
494 Rvs167 recruits Rvs to endocytic sites, effectively increasing the likelihood of BAR domain inter-  
495 action with tubular membrane. BAR domains bind endocytic sites by sensing tubular membrane.

<sup>496</sup> The membrane invagination is stabilized against scission by BAR-membrane interaction. This sta-  
<sup>497</sup> bilization prevents actin-generated forces from rupturing the membrane, and the invaginations  
<sup>498</sup> continue to grow in length as actin continues to polymerize. As actin continues to accumulate,  
<sup>499</sup> pushing forces overcome the resistance to membrane scission. The membrane ruptures, and a  
<sup>500</sup> vesicle is formed.

## <sup>501</sup> Methods and Materials

### <sup>502</sup> Homologous recombination with PCR cassette insertion

<sup>503</sup> Tagging or deletion of endogenous genes was done by homologous integration of the product of a  
<sup>504</sup> Polymerase Chain Reaction (PCR) using appropriate primers and a plasmid containing a selection  
<sup>505</sup> cassette and fluorescent tag, or only selection cassette for gene deletions. Primers were designed  
<sup>506</sup> according to *Janke et al. (2004)*. PCRs used the Velocity Polymerase for fluorescent tagging, and  
<sup>507</sup> Q5 for gene deletions using the NAT cassette. All fluorescently tagged genes have a C-terminus tag  
<sup>508</sup> and are expressed endogenously. Gene deletions and fluorescent tags are checked by PCR. *vps1Δ*  
<sup>509</sup> and gene duplications were confirmed by DNA sequencing.

### <sup>510</sup> Live-cell imaging

#### <sup>511</sup> Sample preparation for live imaging

<sup>512</sup> 40 µL 4mg/ml Concanavalin A (ConA) was incubated on a coverslip for 10 minutes. 40 µL Yeast cells  
<sup>513</sup> incubated overnight at 25°C in imaging medium Synthetic Complete without L-Tryptophan (SC-Trp)  
<sup>514</sup> was added to the coverslip after removing the ConA, and incubated for another 10 minutes. Cells  
<sup>515</sup> were then removed, adhered cells were washed 3x in SC-Trp, and 40 µL SC-TRP was finally added  
<sup>516</sup> to the coverslip to prevent cells from drying.

#### <sup>517</sup> Sample preparation for live imaging in LatA treated cells

<sup>518</sup> Cells went through the same procedure as above till the last washing step. Instead of SC-Trp, 100x  
<sup>519</sup> diluted LatA in SC-Trp was added to the adhered cells . Cells were incubated in LatA for 10 minutes  
<sup>520</sup> before imaging.

#### <sup>521</sup> Epifluorescent imaging for centroid tracking

<sup>522</sup> Live-cell imaging was performed as in (*Picco et al., 2015*). All images were obtained at room temper-  
<sup>523</sup> ature using an Olympus IX81 microscope equipped with a 100×/NA 1.45 PlanApo objective , with  
<sup>524</sup> an additional 1.6x magnification lens and an EMCCD camera. The GFP channel was imaged using  
<sup>525</sup> a 470/22 nm band-pass excitation filter and a 520/35 nm band-pass emission filter. mCherry epi-  
<sup>526</sup> fluorescence imaging was carried out using a 556/20 nm band-pass excitation filter and a 624/40  
<sup>527</sup> band-pass emission filter. GFP was excited using a 488 nm solid state laser and mCherry was  
<sup>528</sup> excited using a 561 nm solid state laser. Hardware was controlled using Metamorph software.  
<sup>529</sup> For single-channel images, 80-120 ms was used as exposure time. All dual-channel images were  
<sup>530</sup> acquired using 250 ms exposure time. Simultaneous dual-color images were obtained using a  
<sup>531</sup> dichroic mirror, with TetraSpeck beads used to correct for chromatic abberation.

**532 Epifluorescent imaging for molecule number quantification**

**533** Images were acquired as in (*Picco et al., 2015*). Z-stacks of cells containing the GFP- or mCherry-  
**534** tagged protein of interest, incubated along with cells containing Nuf2-GFP, were acquired using  
**535** 400 ms exposure using a mercury vapour lamp, on a CCD camera. Z stacks were spaced at 200  
**536** nm.

**537 Live-cell image analysis**

**538** Images were processed for background noise using a rolling ball radius of 90 pixels. Particle de-  
**539** tection, and tracking was performed for a particle size of 6 pixels, using scripts that combine back-  
**540** ground subtraction with Particle Tracker and Detector, that can be found on ImageJ (<http://imagej.nih.gov>).  
**541** Further analysis for centroid averaging, alignments between dual-color images and single channel  
**542** images, for alignment to the reference Abp1 were done using scripts written in Matlab (Mathworks)  
**543** and R ([www.r-project.org](http://www.r-project.org)), written originally by Andrea Picco, and modified by me. Details of anal-  
**544** ysis can be found at (*Picco et al., 2015*). All movement and intensity plots from centroid tracking  
**545** show the average centroid with 95% confidence interval.

**546 Quantification of cytoplasmic concentration**

**547** On a maximum intensity projection of time-lapse images, the average pixel intensity within a circle  
**548** of set radius in the cytoplasm was measured. This circle is manually arranged so that cortical  
**549** patches were excluded, and mean intensity was acquired for about 10 cells of each cell type. A  
**550** fixed area outside the cells was drawn, and mean intensity was calculated to establish "background  
**551** intensity". This background intensity was then subtracted from the mean intensity to obtain a  
**552** rough measure of cytoplasmic intensity.

**553 Acknowledgments**

**554** We would like to thank the entire Kaksonen lab, especially Daniel Hummel, Andrea Picco, and Ma-  
**555** teusz Kozak for critical reading of this manuscript. This work was supported by the Swiss National  
**556** Science Foundation (grant 310030B\_182825) and by the NCCR Chemical Biology funded by the  
**557** SNSF.

**558 References**

- 559** Bensen, E. S., Costaguta, G., and Payne, G. S. (2000). Synthetic genetic interactions with temperature-sensitive  
**560** clathrin in *Saccharomyces cerevisiae*. Roles for synaptojanin-like Inp53p and dynamin-related Vps1p in  
**561** clathrin-dependent protein sorting at the trans-Golgi network. *Genetics*, 154(1):83–97.
- 562** Bieling, P., Li, T.-D., Weichsel, J., Huang, B., Fletcher, D. A., and Dyche Mullins, R. (2016). Force Feedback Controls  
**563** Motor Activity and Mechanical Properties of Self-Assembling Branched Actin Networks. *Cell*, 164:115–127.
- 564** Boeke, D., Trautmann, S., Meurer, M., Wachsmuth, M., Godlee, C., Knop, M., and Kaksonen, M. (2014). Quan-  
**565** tification of cytosolic interactions identifies <scp>E</scp> de1 oligomers as key organizers of endocytosis.  
**566** *Molecular Systems Biology*, 10(11):756.
- 567** Boucrot, E., Pick, A., Camdere, G., Liska, N., Evergren, E., McMahon, H. T., and Kozlov, M. M. (2012). Membrane  
**568** Fission Is Promoted by Insertion of Amphipathic Helices and Is Restricted by Crescent BAR Domains. *Cell*,  
**569** 149(1):124–136.
- 570** Cerveny, K. L., Tamura, Y., Zhang, Z., Jensen, R. E., and Sesaki, H. (2007). Regulation of mitochondrial fusion and  
**571** division. *Trends in Cell Biology*, 17(11):563–569.

- 572 Cestra, G., Castagnoli, L., Dente, L., Minenkova, O., Petrelli, A., Migone, N., Hoffmüller, U., Schneider-Mergener,  
573 J., and Cesareni, G. (1999). The SH3 domains of endophilin and amphiphysin bind to the proline-rich region  
574 of synaptosomal protein 1 at distinct sites that display an unconventional binding specificity. *The Journal of biological  
575 chemistry*, 274(45):32001–7.
- 576 Colwill, K., Field, D., Moore, L., Friesen, J., and Andrews, B. (1999). In Vivo Analysis of the Domains of Yeast  
577 Rvs167p Suggests Rvs167p Function Is Mediated Through Multiple Protein Interactions. *Genetics*, 152(3):881–  
578 893.
- 579 D'Hondt, K., Heese-Peck, A., and Riezman, H. (2000). Protein and Lipid Requirements for Endocytosis. *Annual  
580 Review of Genetics*, 34(1):255–295.
- 581 Dmitrieff, S. and Nédélec, F. (2015). Membrane Mechanics of Endocytosis in Cells with Turgor. *PLoS Comput  
582 Biol*, 11(10):e1004538.
- 583 Farsad, K., Ringstad, N., Takei, K., Floyd, S. R., Rose, K., and De Camilli, P. (2001). Generation of high curvature  
584 membranes mediated by direct endophilin bilayer interactions. *The Journal of Cell Biology*, 155(2):193–200.
- 585 Ferguson, S. M., Brasnjo, G., Hayashi, M., Wölfel, M., Collesi, C., Giovedi, S., Raimondi, A., Gong, L. W., Ariel, P., Par-  
586 adise, S., O'Toole, E., Flavell, R., Cremona, O., Miesenböck, G., Ryan, T. A., and De Camilli, P. (2007). A selective  
587 activity-dependent requirement for dynamin 1 in synaptic vesicle endocytosis. *Science*, 316(5824):570–574.
- 588 Ferguson, S. M., Raimondi, A., Paradise, S., Shen, H., Mesaki, K., Ferguson, A., Destaing, O., Ko, G., Takasaki, J.,  
589 Cremona, O., O'Toole, E., and De Camilli, P. (2009). Coordinated actions of actin and BAR proteins upstream  
590 of dynamin at endocytic clathrin-coated pits. *Developmental cell*, 17(6):811–822.
- 591 Friesen, H., Humphries, C., Ho, Y., Schub, O., Colwill, K., and Andrews, B. (2006). Characterization of the Yeast  
592 Amphiphysins Rvs161p and Rvs167p Reveals Roles for the Rvs Heterodimer In Vivo. *Molecular Biology of the  
593 Cell*, 17(3):1306–1321.
- 594 Galli, V., Sebastian, R., Moutel, S., Ecard, J., Perez, F., and Roux, A. (2017). Uncoupling of dynamin polymerization  
595 and GTPase activity revealed by the conformation-specific nanobody dynab. *eLife*, 6:e25197.
- 596 Goud Gadila, S. K., Williams, M., Saimani, U., Delgado Cruz, M., Makaraci, P., Woodman, S., Short, J. C., McDer-  
597 mott, H., and Kim, K. (2017). Yeast dynamin Vps1 associates with clathrin to facilitate vesicular trafficking  
598 and controls Golgi homeostasis. *European Journal of Cell Biology*, 96(2):182–197.
- 599 Grabs, D., Slepnev, V. I., Songyang, Z., David, C., Lynch, M., Cantley, L. C., and De Camilli, P. (1997). The SH3  
600 domain of amphiphysin binds the proline-rich domain of dynamin at a single site that defines a new SH3  
601 binding consensus sequence. *The Journal of biological chemistry*, 272(20):13419–25.
- 602 Grigliatti, T. A., Hall, L., Rosenbluth, R., and Suzuki, D. T. (1973). Temperature-Sensitive Mutations in *Drosophila*  
603 *melanogaster* XIV. A Selection of Immobile Adults \*. *Molec. gen. Genet.*, 120:107–114.
- 604 Gurunathan, S., David, D., and Gerst, J. E. (2002). Dynamin and clathrin are required for the biogenesis of a  
605 distinct class of secretory vesicles in yeast. *The EMBO journal*, 21(4):602–14.
- 606 Hoepfner, D., van den Berg, M., Philippse, P., Tabak, H. F., and Hettema, E. H. (2001). A role for Vps1p, actin,  
607 and the Myo2p motor in peroxisome abundance and inheritance in *< i>Saccharomyces cerevisiae</i>*. *The  
608 Journal of Cell Biology*, 155(6):979–990.
- 609 Huber, F., Meurer, M., Bunina, D., Kats, I., Maeder, C. I., Štefl, M., Mongis, C., and Knop, M. (2014). PCR Dupli-  
610 cation: A One-Step Cloning-Free Method to Generate Duplicated Chromosomal Loci and Interference-Free  
611 Expression Reporters in Yeast. *PLoS ONE*, 9(12):e114590.
- 612 Janke, C., Magiera, M. M., Rathfelder, N., Taxis, C., Reber, S., Maekawa, H., Moreno-Borchart, A., Doenges, G.,  
613 Schwob, E., Schieberl, E., and Knop, M. (2004). A versatile toolbox for PCR-based tagging of yeast genes:  
614 new fluorescent proteins, more markers and promoter substitution cassettes. *Yeast (Chichester, England)*,  
615 21(11):947–962.
- 616 Joglekar, A. P., Bouck, D. C., Molk, J. N., Bloom, K. S., and Salmon, E. D. (2006). Molecular architecture of a  
617 kinetochore-microtubule attachment site. *Nature Cell Biology*, 8(6):581–585.
- 618 Kaksonen, M. and Roux, A. (2018). Mechanisms of clathrin-mediated endocytosis.
- 619 Kaksonen, M., Sun, Y., and Drubin, D. G. (2003). A pathway for association of receptors, adaptors, and actin  
620 during endocytic internalization. *Cell*, 115(4):475–487.

- 621 Kaksonen, M., Toret, C. P., and Drubin, D. G. (2005). A modular design for the clathrin- and actin-mediated  
622 endocytosis machinery. *Cell*, 123(2):305–320.
- 623 Kishimoto, T., Sun, Y., Buser, C., Liu, J., Michelot, A., and Drubin, D. G. (2011). Determinants of endocytic mem-  
624 brane geometry, stability, and scission. *Proceedings of the National Academy of Sciences of the United States of*  
625 *America*, 108(44):E979–E988.
- 626 Kübler, E., Riezman, H., Riezman, H., and Riezman, H. (1993). Actin and fimbrin are required for the internaliza-  
627 tion step of endocytosis in yeast. *The EMBO journal*, 12(7):2855–62.
- 628 Kukulski, W., Schorb, M., Kaksonen, M., and Briggs, J. G. (2012). Plasma Membrane Reshaping during Endocy-  
629 tosis Is Revealed by Time-Resolved Electron Tomography. *Cell*, 150(3):508–520.
- 630 Lila, T. and Drubin, D. G. (1997). Evidence for physical and functional interactions among two *Saccharomyces*  
631 *cerevisiae* SH3 domain proteins, an adenylyl cyclase-associated protein and the actin cytoskeleton. *Molecular*  
632 *Biology of the Cell*, 8(2):367–385.
- 633 Liu, J., Sun, Y., Drubin, D. G., and Oster, G. F. (2009). The Mechanochemistry of Endocytosis. *PLoS Biol*,  
634 7(9):e1000204.
- 635 Lombardi, R. and Riezman, H. (2001). Rvs161p and Rvs167p, the Two Yeast Amphiphysin Homologs, Function  
636 Together in Vivo. *Journal of Biological Chemistry*, 276(8):6016–6022.
- 637 Madania, A., Dumoulin, P., Grava, S., Kitamoto, H., Scharer-Brodbeck, C., Soulard, A., Moreau, V., and Winsor,  
638 B. (1999). The *Saccharomyces cerevisiae* Homologue of Human Wiskott-Aldrich Syndrome Protein Las17p  
639 Interacts with the Arp2/3 Complex. *Molecular Biology of the Cell*, 10(10):3521–3538.
- 640 McMahon, H. T. and Boucrot, E. (2011). Molecular mechanism and physiological functions of clathrin-mediated  
641 endocytosis.
- 642 McPherson, P. S., Garcia, E. P., Slepnev, V. I., David, C., Zhang, X., Grabs, D., Sossini, W. S., Bauerfeind, R., Nemoto,  
643 Y., and De Camilli, P. (1996). A presynaptic inositol-5-phosphatase. *Nature*, 379(6563):353–357.
- 644 Meinecke, M., Boucrot, E., Camdere, G., Hon, W.-C., Mittal, R., and McMahon, H. T. (2013). Cooperative re-  
645 cruitment of dynamin and BIN/amphiphysin/Rvs (BAR) domain-containing proteins leads to GTP-dependent  
646 membrane scission. *The Journal of biological chemistry*, 288(9):6651–61.
- 647 Mim, C., Cui, H., Gawronski-Salerno, J. A., Frost, A., Lyman, E., Voth, G. A., and Unger, V. M. (2012). Structural  
648 basis of membrane bending by the N-BAR protein endophilin. *Cell*, 149(1):137–145.
- 649 Munn, A. L., Stevenson, B. J., Gelli, M. I., and Riezman, H. (1995). end5, end6, and end7: Mutations that cause  
650 actin delocalization and block the internalization step of endocytosis in *Saccharomyces cerevisiae*. *Molecular*  
651 *Biology of the Cell*, 6(12):1721–1742.
- 652 Nannapaneni, S., Wang, D., Jain, S., Schroeder, B., Highfill, C., Reustle, L., Pittsley, D., Maysent, A., Moulder, S.,  
653 McDowell, R., and Kim, K. (2010). The yeast dynamin-like protein Vps1:vps1 mutations perturb the internal-  
654 ization and the motility of endocytic vesicles and endosomes via disorganization of the actin cytoskeleton.  
655 *European Journal of Cell Biology*, 89(7):499–508.
- 656 Nothwehr, S. F., Conibear, E., and Stevens, T. H. (1995). Golgi and vacuolar membrane proteins reach the  
657 vacuole in vps1 mutant yeast cells via the plasma membrane. *The Journal of Cell Biology*, 129(1):35–46.
- 658 Peter, B. J., Kent, H. M., Mills, I. G., Vallis, Y., Butler, P. J. G., Evans, P. R., and McMahon, H. T. (2004). BAR Domains  
659 as Sensors of Membrane Curvature: The Amphiphysin BAR Structure. *Science*, 303(5657):495–499.
- 660 Peters, C., Baars, T. L., Bühler, S., and Mayer, A. (2004). Mutual control of membrane fission and fusion proteins.  
661 *Cell*, 119(5):667–78.
- 662 Picco, A., Kukulski, W., Manenschijn, H. E., Specht, T., Briggs, J. A. G., and Kaksonen, M. (2018). The contributions  
663 of the actin machinery to endocytic membrane bending and vesicle formation. *Molecular Biology of the Cell*,  
664 29(11):1346–1358.
- 665 Picco, A., Mund, M., Ries, J., Nédélec, F., and Kaksonen, M. (2015). Visualizing the functional architecture of the  
666 endocytic machinery. *eLife*, page e04535.
- 667 Rooij, I. I. S.-d., Allwood, E. G., Aghamohammadzadeh, S., Hettema, E. H., Goldberg, M. W., and Ayscough,  
668 K. R. (2010). A role for the dynamin-like protein Vps1 during endocytosis in yeast. *Journal of Cell Science*,  
669 123(20):3496–3506.

- 670 Rothman', J. H., Howald, I., and Stevens, T. H. (1989). Characterization of genes required for protein sorting and  
671 vacuolar function in the yeast *Saccharomyces cerevisiae*. Technical Report 7.
- 672 Rothman, J. H., Raymond, C. K., Gilbert, T., O'Hara, P. J., and Stevens, T. H. (1990). A putative GTP binding protein  
673 homologous to interferon-inducible Mx proteins performs an essential function in yeast protein sorting. *Cell*,  
674 61(6):1063-1074.
- 675 Rothman, J. I. and Stevens, T. H. (1986). Protein Sorting in Yeast: Mutants Defective in Vacuole Biogenesis  
676 Mislocalize Vacuolar Proteins into the Late Secretory Pathway. Technical report.
- 677 Shupliakov, O., Löw, P., Grabs, D., Gad, H., Chen, H., David, C., Takei, K., De Camilli, P., and Brodin, L. (1997).  
678 Synaptic vesicle endocytosis impaired by disruption of dynamin-SH3 domain interactions. *Science (New York,*  
679 *N.Y.*, 276(5310):259-63.
- 680 Simunovic, M., Manneville, J.-B., Renard, H.-F. O., Johannes, L., Bassereau, P., Callan, A., Correspondence, J.,  
681 Evergren, E., Raghunathan, K., Bhatia, D., Kenworthy, A. K., Voth, G. A., Prost, J., McMahon, H. T., and Callan-  
682 Jones, A. (2017). Friction Mediates Scission of Tubular Membranes Scaffolded by BAR Proteins. *Cell*, 170:1-13.
- 683 Singer-Krüger, B., Nemoto, Y., Daniell, L., Ferro-Novick, S., and De Camilli, P. (1998). Synaptojanin family mem-  
684 bers are implicated in endocytic membrane traffic in yeast. *Journal of cell science*, 111 ( Pt 2):3347-3356.
- 685 Sivadon, P., Crouzet, M., and Aigle, M. (1997). Functional assessment of the yeast Rvs161 and Rvs167 protein  
686 domains. *FEBS letters*, 417(1):21-27.
- 687 Skruzny, M., Brach, T., Ciuffa, R., Rybina, S., Wachsmuth, M., and Kaksonen, M. (2012). Molecular basis for  
688 coupling the plasma membrane to the actin cytoskeleton during clathrin-mediated endocytosis. *Proceedings  
689 of the National Academy of Sciences of the United States of America*, 109(38):E2533-42.
- 690 Smaczynska-de Rooij, I. I., Allwood, E. G., Mishra, R., Booth, W. I., Aghamohammazadeh, S., Goldberg, M. W.,  
691 and Ayscough, K. R. (2012). Yeast Dynamin Vps1 and Amphiphysin Rvs167 Function Together During Endo-  
692 cytosis. *Traffic*, 13(2):317-328.
- 693 Stoltz, L. E., Huynh, C. V., Thorner, J., and York, J. D. (1998a). Identification and characterization of an essen-  
694 tial family of inositol polyphosphate 5-phosphatases (INP51, INP52 and INP53 gene products) in the yeast  
695 *Saccharomyces cerevisiae*. *Genetics*, 148(4):1715-29.
- 696 Stoltz, L. E., Kuo, W. J., Longchamps, J., Sekhon, M. K., and York, J. D. (1998b). INP51, a yeast inositol polyphos-  
697 phate 5-phosphatase required for phosphatidylinositol 4,5-bisphosphate homeostasis and whose absence  
698 confers a cold-resistant phenotype. *The Journal of biological chemistry*, 273(19):11852-61.
- 699 Sun, Y., Carroll, S., Kaksonen, M., Toshima, J. Y., and Drubin, D. G. (2007). PtdIns(4,5)P2 turnover is required  
700 for multiple stages during clathrin- and actin-dependent endocytic internalization. *The Journal of Cell Biology*,  
701 177(2):355-367.
- 702 Sweitzer, S. M. and Hinshaw, J. E. (1998). Dynamin Undergoes a GTP-Dependent Conformational Change Caus-  
703 ing Vesiculation. *Cell*, 93(6):1021-1029.
- 704 Takei, K., McPherson, P. S., Schmid, S. L., and Camilli, P. D. (1995). Tubular membrane invaginations coated by  
705 dynamin rings are induced by GTP-γS in nerve terminals. *Nature*, 374(6518):186-190.
- 706 Theriot, J. A., Mitchison, T. J., Tilney, L. G., and Portnoy, D. A. (1992). The rate of actin-based motility of intracel-  
707 lular *Listeria monocytogenes* equals the rate of actin polymerization. *Nature*, 357(6375):257-260.
- 708 Toret, C. P., Lee, L., Sekiya-Kawasaki, M., and Drubin, D. G. (2008). Multiple Pathways Regulate Endocytic Coat  
709 Disassembly in *Saccharomyces cerevisiae* for Optimal Downstream Trafficking. *Traffic*, 9(5):848-859.
- 710 Watanabe, S., Mamer, L. E., Raychaudhuri, S., Luvsanjav, D., Eisen, J., Trimbuch, T., Söhl-Kielczynski, B., Fenske,  
711 P., Milosevic, I., Rosenmund, C., and Jorgensen, E. M. (2018). Synaptojanin and Endophilin Mediate Neck  
712 Formation during Ultrafast Endocytosis. *Neuron*, 98(6):1184-1197.e6.
- 713 Youn, J.-Y., Friesen, H., Kishimoto, T., Henne, W. M., Kurat, C. F., Ye, W., Ceccarelli, D. F., Sicheri, F., Kohlwein,  
714 S. D., McMahon, H. T., and Andrews, B. J. (2010). Dissecting BAR Domain Function in the Yeast Amphiphysins  
715 Rvs161 and Rvs167 during Endocytosis. *Molecular Biology of the Cell*, 21(17):3054-3069.
- 716 Yu, X. and Cai, M. (2004). The yeast dynamin-related GTPase Vps1p functions in the organization of the actin  
717 cytoskeleton via interaction with Sla1p. *Journal of Cell Science*, 117(17):3839-3853.

- <sup>718</sup> Zhang, P. and Hinshaw, J. E. (2001). Three-dimensional reconstruction of dynamin in the constricted state.  
<sup>719</sup> *Nature Cell Biology*, 3(10):922–926.
- <sup>720</sup> Zhao, H., Michelot, A., Koskela, E. V., Tkach, V., Stamou, D., Drubin, D. G., and Lappalainen, P. (2013). Membrane-  
<sup>721</sup> Sculpting BAR Domains Generate Stable Lipid Microdomains. *Cell Reports*, 4:1213–1223.
- <sup>722</sup> Zhao, W.-D., Hamid, E., Shin, W., Wen, P. J., Krystofiak, E. S., Villarreal, S. A., Chiang, H.-C., Kachar, B., and Wu, L.-G.  
<sup>723</sup> (2016). Hemi-fused structure mediates and controls fusion and fission in live cells. *Nature*, 534(7608):548–52.

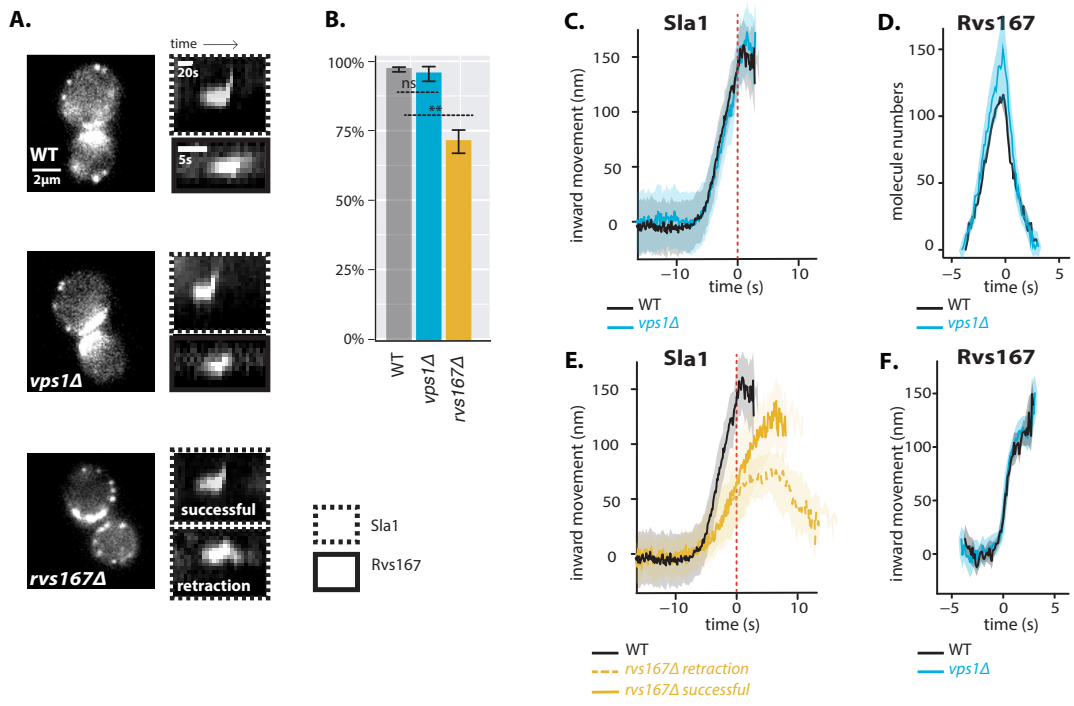


**Figure 1. *vps1* $\Delta$  and *rvs167* $\Delta$  deletion.** **A:** Left: Single frames from time-lapse movies of WT, *vps1* $\Delta$ , and *rvs167* $\Delta$  cells with endogenously tagged Sla1-eGFP. Right: Kymographs of WT, *vps1* $\Delta$ , and *rvs167* $\Delta$  cells tagged with Sla1-eGFP or Rvs167-eGFP. **B:** Scission efficiency in WT, *vps1* $\Delta$ , and *rvs167* $\Delta$  cells. Error bars are standard deviation, p values from two-sided t-test, \* $= p \leq 0.05$ , \*\* $= p \leq 0.01$ , \*\*\* $= p \leq 0.001$ . **C:** Averaged centroid positions of Sla1-eGFP in WT and *vps1* $\Delta$  cells. **D:** Number of Rvs167 molecules in WT and *vps1* $\Delta$  cells. **E:** Averaged centroid positions of Sla1-eGFP in WT, and successful and retracted Sla1-eGFP positions in *rvs167* $\Delta$  cells. **F:** Averaged centroid positions of Rvs167-eGFP in WT and *vps1* $\Delta$  cells. All centroids were aligned in x-axis so that time=0 s corresponds to Abp1 intensity maximum. Centroids were aligned in the y-axis to a starting position = 0 nm. Shading on plots show 95% confidence intervals. Dashed red lines indicate Abp1 intensity maxima.

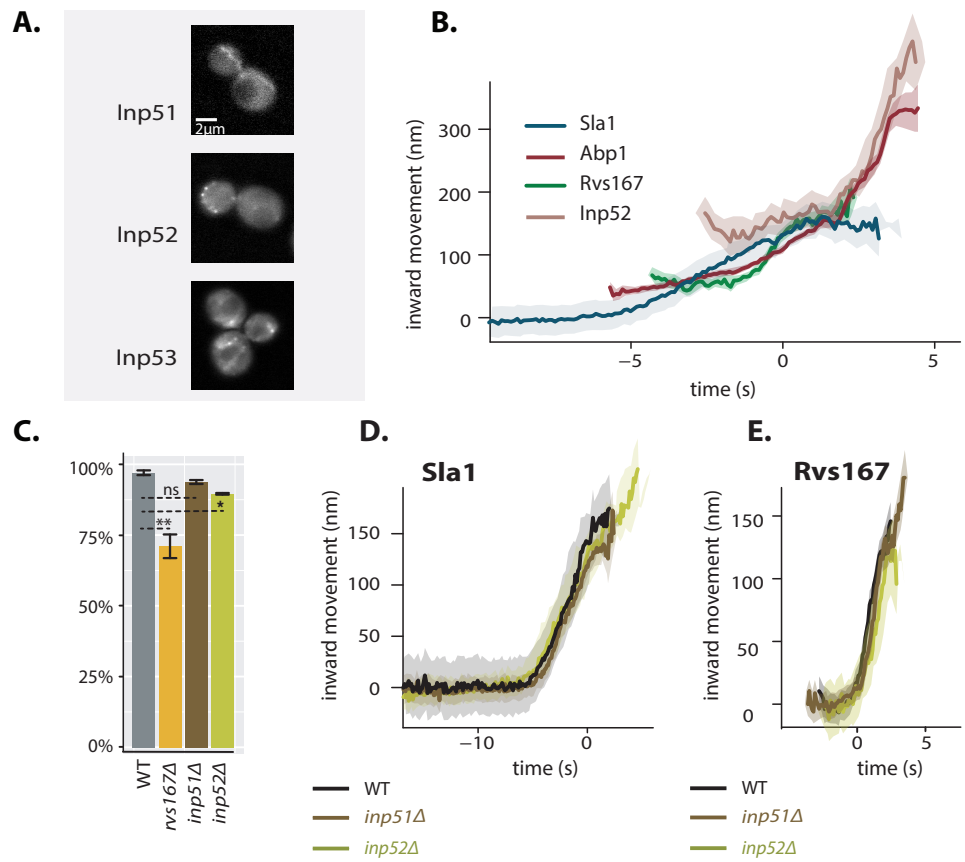


**Figure 2. Yeast synaptojanin-like proteins in endocytosis. A:** Cells with endogenously tagged Inp51-, Inp52-, and Inp53-eGFP. **B:** Inp52 centroid trajectory aligned in space and time to other endocytic proteins. **C:** Scission efficiency in WT, *rvs167Δ*, *inp51Δ*, and *inp52Δ* cells. Error bars are standard deviation, with p values from two-sided t-test; \* $p \leq 0.05$ , \*\* $p \leq 0.01$ , \*\*\* $p \leq 0.001$ . **D:** Averaged centroid positions of Sla1-eGFP in WT, *inp51Δ*, and *inp52Δ* cells. **E:** Averaged centroid positions of Rvs167-eGFP in WT, *inp51Δ*, and *inp52Δ* cells. All centroid positions were aligned in x-axis so that time=0 s corresponds to Abp1 intensity maximum. Centroids were aligned in the y-axis to a starting position = 0 nm. Shading on plots represent 95% confidence interval.

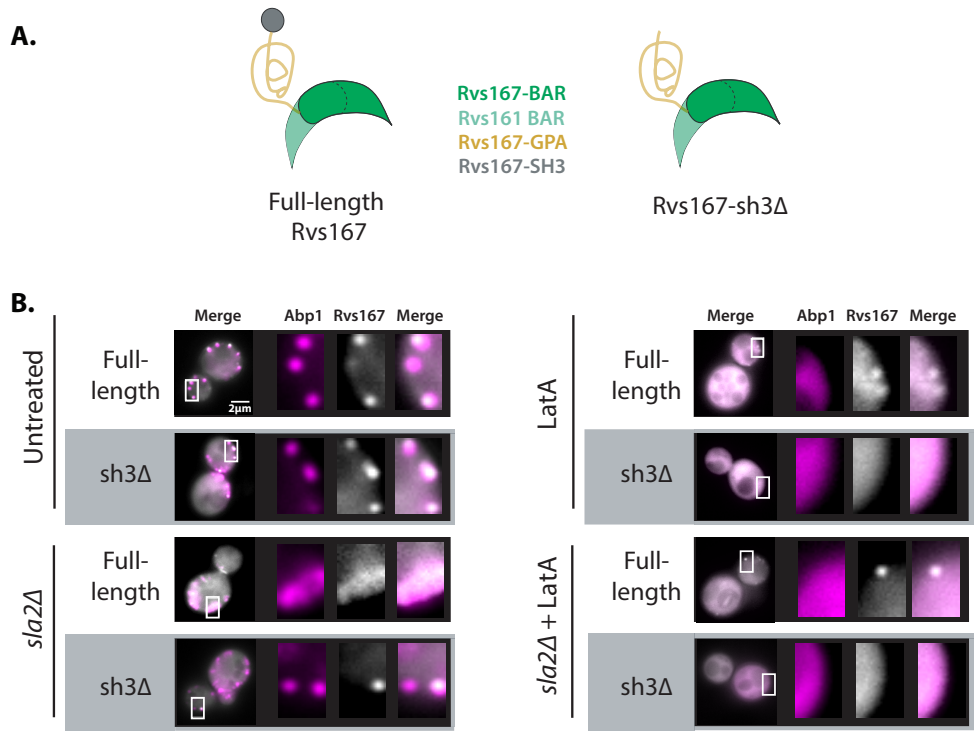


**Figure 3. Localization of Rvs167 BAR domain. A:** Schematic of Rvs protein complex with and without the SH3 domain. **B:** Localization of full-length Rvs167 and Rvs167-sh3Δ in WT, *sla2Δ*, LatA treated, and LatA treated *sla2Δ* cells.

### Rvs167-eGFP

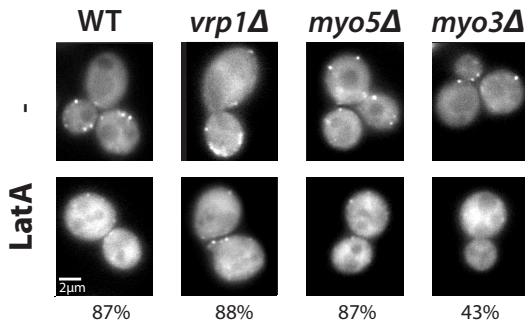


**Figure 4. Localization of Rvs167 in the absence of membrane curvature.** Single frames from time-lapse movies showing Rvs167-eGFP localization in untreated and LatA treated WT, *vrp1Δ*, *myo5Δ*, and *myo3Δ* cells. Percentages indicate number of LatA treated cells in which Rvs167-eGFP is localized at the plasma membrane.

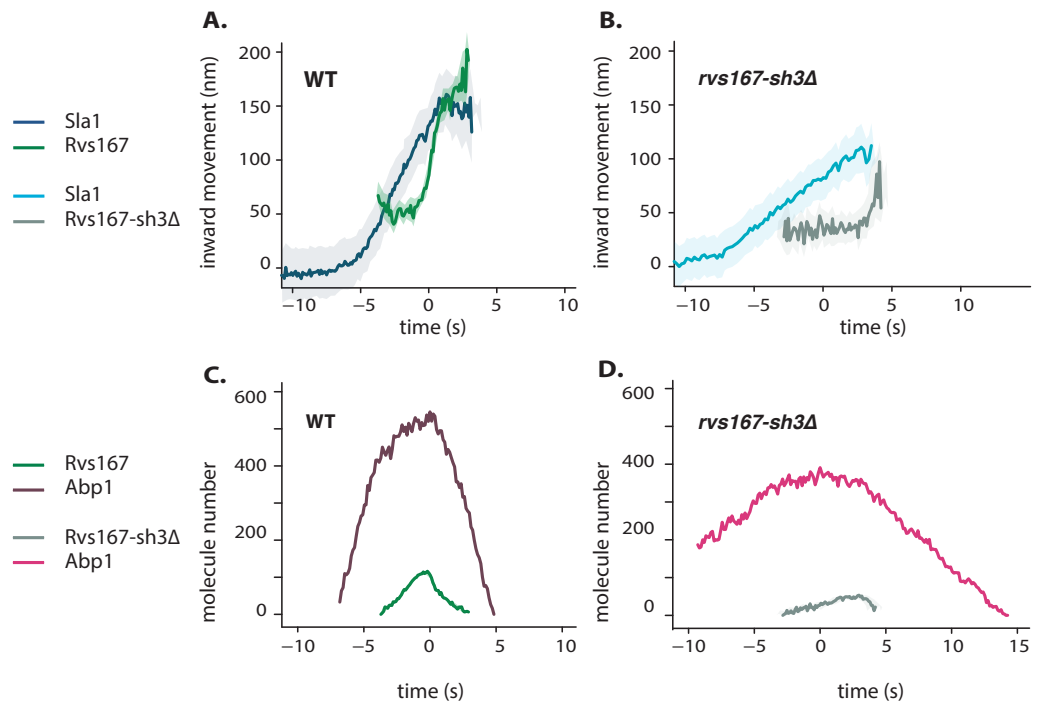


**Figure 5. Endocytic dynamics in *rvs167-sh3Δ* cells. A,B:** Averaged centroid positions aligned in x-axis so that time=0 s corresponds to Abp1 intensity maximum in the respective strains. Centroids were aligned in y-axis so that non-motile Sla1 position is at y=0 nm, and Rvs167 and Rvs167-sh3Δ positions are determined with respect to Sla1 centroids. **C,D:** Numbers of molecules in WT and *rvs167-sh3Δ* cells, aligned so that time=0 s is the Abp1 intensity maximum in the corresponding strains. Shading represents 95% confidence interval.

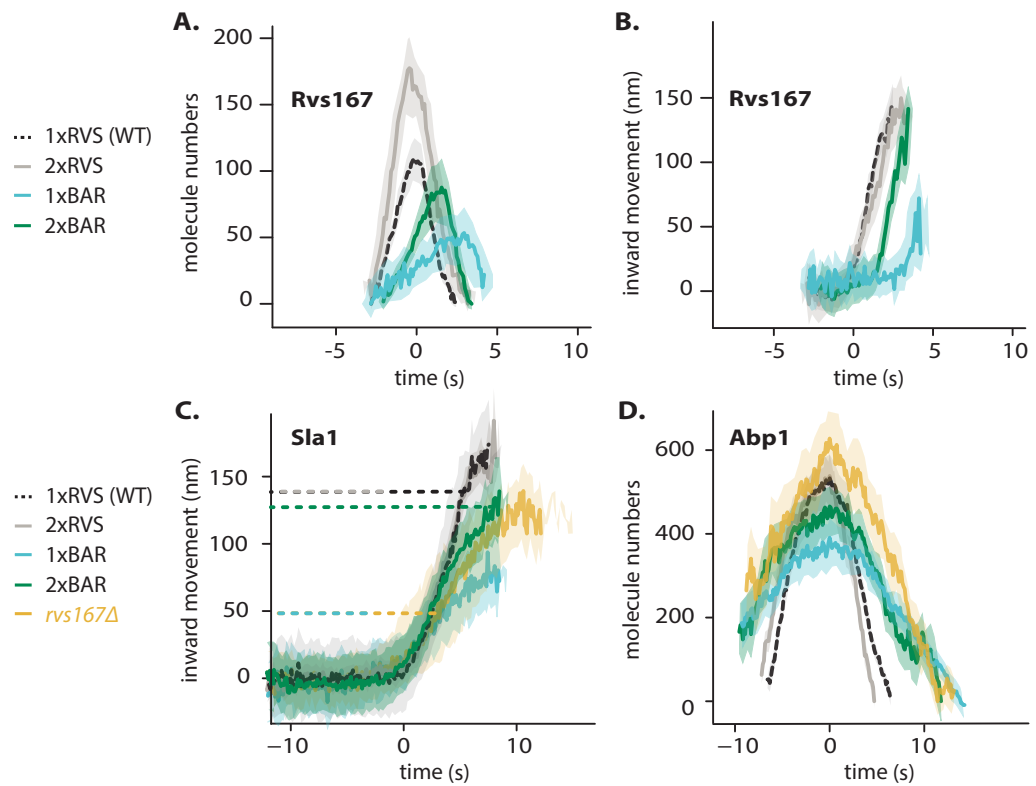


**Figure 6. Titration of BAR molecules.** **A,B:** Molecule numbers and centroid positions of Rvs167. Centroid positions were aligned in x-axis so that time=0 s corresponds to Abp1 intensity maximum. Centroids movements were aligned in the y-axis to a starting position = 0 nm. **C:** Sla1 centroid positions, aligned so that the centroids begin inwards movement at the same time. Aligned in the y-axis so that y=0 nm corresponds to the beginning of the average centroid position. Dashed lines correspond to the Sla1 centroid positions when intensity of Abp1 in the corresponding strain is at maximum. **D:** Abp1 molecule number, aligned in x-axis so that time=0 s corresponds to Abp1 intensity maximum

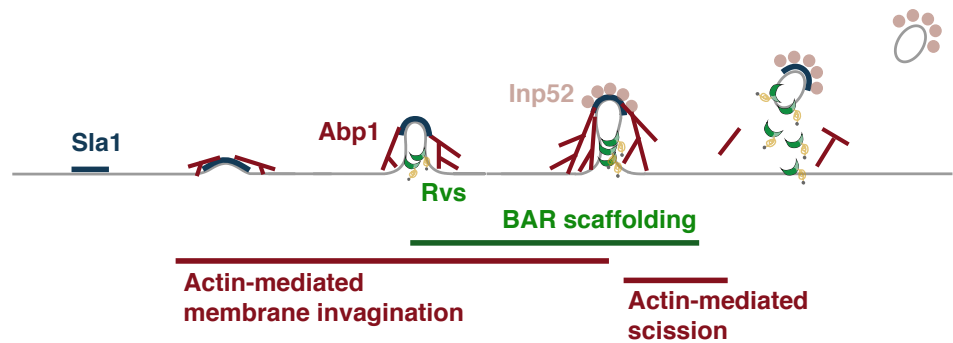


**Figure 7. Model for yeast endocytic scission.** Membrane at an endocytic site is bent by forces derived from actin polymerization. BAR domains arrive at a tubular invagination and scaffold the membrane, delaying scission. Actin forces eventually overcome the influence of BAR scaffolding, and the membrane breaks, resulting in vesicle formation.

724 **Supplementary Material**

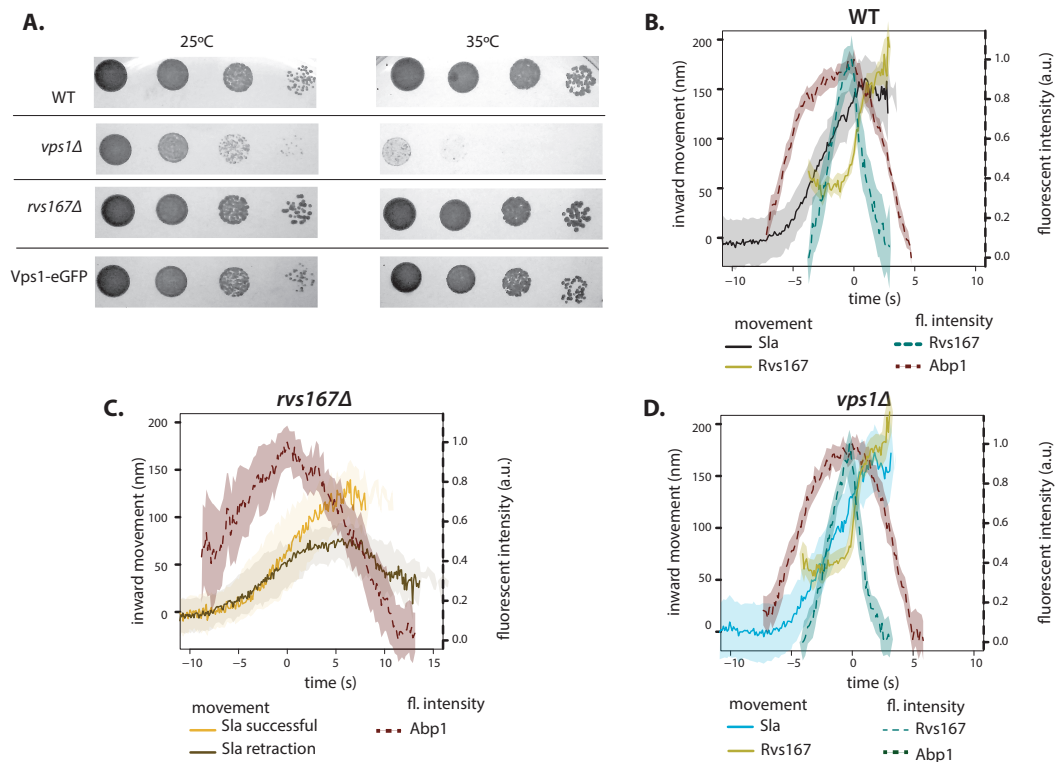


**Figure S1. A:** Growth assay of WT, *vps1* $\Delta$ , *rvs167* $\Delta$ , and cells expressing Vps1-eGFP at 25°C and 35°C . **B, C, D:** Sla1 and Rvs167 centroids aligned so that time=0 s is the maximum of Abp1 fluorescent intensity. Centroid movements aligned so that y=0 nm is the starting Sla1 position. Normalized Abp1 and Rvs167 fluorescent intensities in WT, *vps1* $\Delta$ , and *rvs167* $\Delta$  cells.

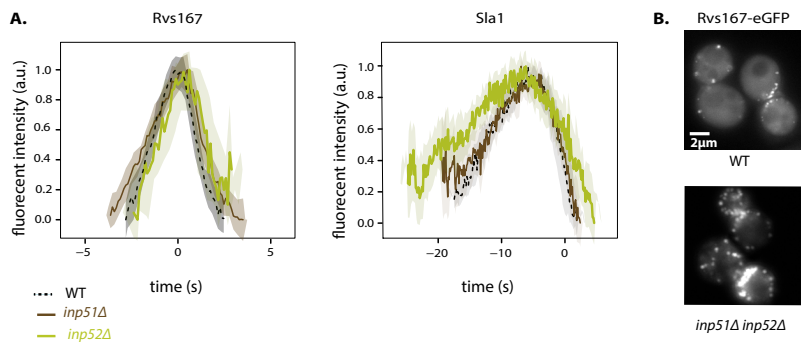


**Figure S2. A:** Normalized Rvs167 and Sla1 fluorescent intensities in synaptojanin deletion aligned in time so that time=0 s corresponds to Abp1 intensity maximum. **B:** Maximum intensity projection of a time-lapse movie of Rvs167-eGFP in WT and *inp51Δ**inp52Δ* cells.

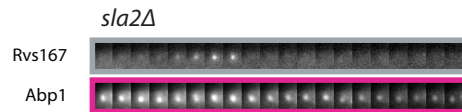


**Figure S3.** Rvs167-eGFP and Abp1-mCherry in *sla2Δ* cells

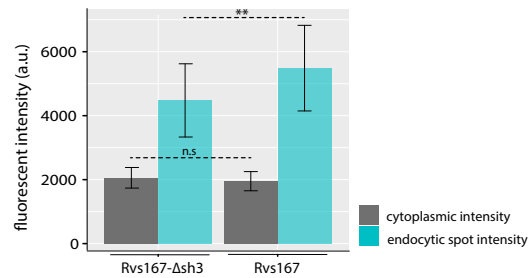


**Figure S4.** Cytoplasmic intensity and intensity of endocytic patches of Rvs167-eGFP and Rvs167-sh3Δ-eGFP. Error bars are standard deviation, p values from two-sided t-test, \* =  $p \leq 0.05$ , \*\* =  $p \leq 0.01$ , \*\*\* =  $p \leq 0.001$ .

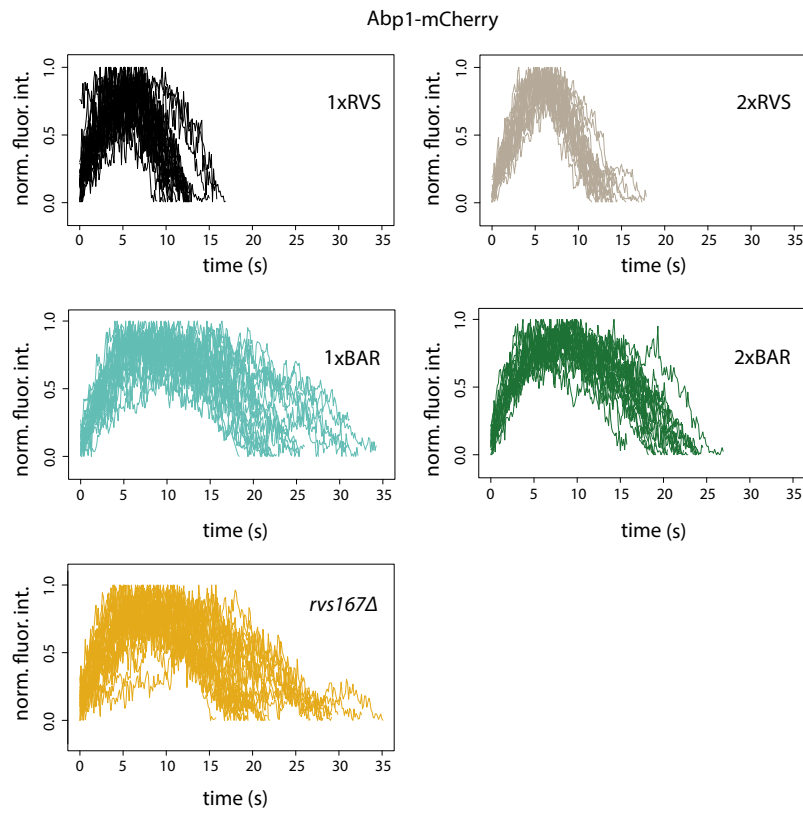


**Figure S5.** Normalized fluorescent intensities of Abp1-mCherry in 1xRVS, 2xRVS, 1xBAR, 2xBAR and *rvs167Δ* cells co-tagged with Sla1-eGFP

STRAIN	% Sla1 retraction	Max. Rvs167#	Max. Abp1#
1xRVS (WT)	2.4	$109.5 \pm 5.2$	$538.3 \pm 27.8$
2xRVS	7.2	$177.5 \pm 7.5$	$533.3 \pm 28.1$
1xBAR	10.4	$53.4 \pm 9.9$	$390.9 \pm 24.6$
2xBAR	10.7	$87.6 \pm 9.6$	$465.5 \pm 25$
<i>rvs167Δ</i>	28.8	-	$627.7 \pm 39.36$
<i>inp51Δ</i>	6.25	$119.1 \pm 5$	$491.6 \pm 33.9$
<i>inp52Δ</i>	10.42	$105.7 \pm 7.1$	$513.6 \pm 50$

**Figure S6. Percentage of retracting events, Rvs167 and Abp1 molecule numbers**